HEAT FLUX AND EFFECTIVENESS IN BUBBLE COLUMN DEHUMIDIFIERS FOR HDH DESALINATION

Authors: *E. W. Tow, J. H. Lienhard V*

Presenter: Emily W. Tow
SM Candidate – Massachusetts Institute of Technology – USA
emilytow@mit.edu

Abstract

Humidification-dehumidification is a promising technology for decentralized, small-scale desalination, but high energy consumption and large dehumidifier size are disadvantages. Direct-contact dehumidification in bubble columns has previously been shown to decrease dehumidifier volume by an order of magnitude. In a bubble column dehumidifier, warm, moist air is bubbled though a column of fresh water cooled by heat exchange with seawater feed. The concentration gradient from the warm bubble center to the cool bubble surface drives radial mass diffusion, and water vapor condenses on the surface of the bubble. In this paper, a parallel-flow effectiveness is defined to complement heat flux when assessing the performance of a single-stage bubble column dehumidifier. A bubble column dehumidifier is tested using significantly smaller cooling coils than those tested in previous work. Experimental results are presented in terms of heat flux and effectiveness in order to better understand the factors influencing bubble column dehumidifier performance. It is found that the heat flux can be raised dramatically by reducing the coil area, but that this gain is accompanied by a loss of effectiveness. Increasing air temperature leads to increased heat flux but decreased effectiveness. Because the gas-side pressure drop increases with increasing column liquid height, significantly lower column liquid heights are tested than those used in previous work. The critical liquid height is found to be below 4 cm for the sparger and flow rate tested. Additional heat transfer in the air gap is explored, but found to be minimal for well-designed columns with low temperature pinch. These findings will inform the design of bubble column dehumidifiers for high heat recovery and low capital cost.

I. INTRODUCTION

Humidification-dehumidification (HDH) is a promising method for decentralized, small-scale desalination because of its simple system design and compatibility with low-grade energy [1]. In its most basic form, a HDH system consists of a heater, a humidifier, a dehumidifier, and the pumps and piping necessary to move fluid between components. Some implementations such as natural convection HDH are particularly simple in design, but some more complex configurations, several of which are described in [2], have the potential for higher energy recovery [3]. To increase efficiency and reduce capital cost, dehumidification technology warrants further study because of the high condenser area required to overcome the resistance to diffusion of a dilute vapor through air, and because the effectiveness of the dehumidifier dominates the performance of the entire system [4].

Direct-contact dehumidification in bubble columns has previously been shown to reduce dehumidifier size by an order of magnitude [5]. A schematic diagram of the bubble column dehumidifier used in this work is shown in Figure 1. In a bubble column dehumidifier, warm, moist air is bubbled though a column of fresh water cooled by indirect heat exchange with seawater. The concentration gradient from the warm bubble center to the cool bubble interface drives condensation on the surface of the bubble. Narayan et al. [2] noted that some proposed direct-contact dehumidification schemes [6] were undesirable in HDH systems due to poor heat recovery; however, a bubble column dehumidifier recovers heat by using seawater as a coolant in the dehumidifier, thereby preheating it for use in the humidifier. Multistage bubble columns further enhance this energy recovery [7].
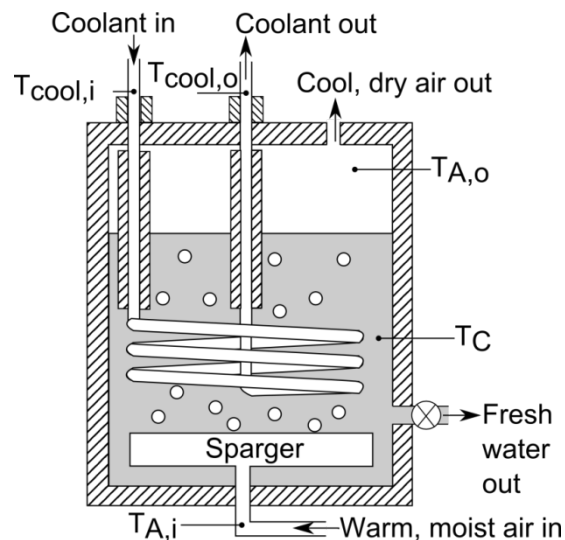

Figure 1: Schematic diagram of the experimental dehumidifier.

The heat and mass transfer processes in bubble column dehumidifiers are not yet well characterized. Bubble column reactors have been studied extensively as gas-liquid reactors where the mass diffusion resistance between the bubble surface and the bulk liquid dominates the performance of the column [8]. Additionally, several researchers have noted that the gas and liquid phases behave differently near the gas inlet [8-11]. However, most bubble column reactors are significantly taller than those used for dehumidification [5,8], so the entry region is often neglected in the reactor modeling and design literature. A model by Narayan et al. proposes a thermal resistance network for the bubble column

dehumidifier with transport mechanisms taken from the bubble column reactor literature [5]. This model predicts the heat flux with reasonable accuracy in simple configurations, but it calls for refinement. Another model [12] proposes a different resistance network along with mean heat and mass transfer driving forces in the bubble stream, but does not predict heat and mass transfer coefficients. The results presented in the present paper can be used to validate future transport modeling and to enable improvements in HDH system modeling and optimization.

Because the cost of a bubble column dehumidifier is strongly influenced by the mass of copper used in the coil, the experiment performed in this work uses much shorter cooling coils than those used by Narayan et al. [5] with the aim of achieving higher coil-surface heat fluxes. However, changes to the column design (e.g. coil length) or operation (e.g. moist air temperature) that increase the heat flux may reduce capital cost, but may also reduce the effectiveness of the dehumidifier. By defining a parallel-flow effectiveness, the effect of changes to the column design and operation can be quantified in terms of heat flux and effectiveness to give insight into both capital and energy costs.

II.   NOMENCLATURE

D	Diameter [m]
g	Gravitational acceleration [m/s^2]
h	Specific enthalpy [J/kg]
h_{fg}	Latent heat of vaporization [J/kg]
m	Mass fraction [-]
$\dot{m}$	Mass flow rate [kg/s]
M	Molar mass [kg/kmol]
N	Number [-]
P	Absolute pressure [Pa]
$\dot{Q}$	Heat transfer rate [W]
R	Thermal resistance [K/W]
Re	Reynolds number [-]
T	Temperature [C]
u	Average velocity [m/s]

Greek
ε	Effectiveness [-]
μ	Viscosity [Pa-s]
σ	Surface tension [N/m]
ρ	Density [kg/m^3]

Subscripts
//	Parallel-flow
A	Moist gas stream
a	Dry air
B	Bubble inner surface
b	Bubble
C	Column fluid
$cond$	Condensation
D	Coil

E   Coolant
f   Liquid water
g   Water vapor
h   Sparger orifice
i   In
ma   Moist air
max   Maximum
meas   Measured
o   Out
sat   Saturation

III.   THEORY

To analyze the experimental results, a resistance model will be proposed and a parallel-flow effectiveness will be defined based on the maximum heat transfer rate of a single stage.

3.1   Resistance Network Model

The following resistance network governing heat and water vapor mass transfer in the liquid portion of a steady-state bubble column dehumidifier is shown in Figure 2. This revisits the work of Narayan et al. [5] but separates the column into two thermal boundary layers and eliminates an unphysical mass transfer resistance outside the bubble (see [13]). The "bubble-on-coil impact" resistance and associated current source are also removed.
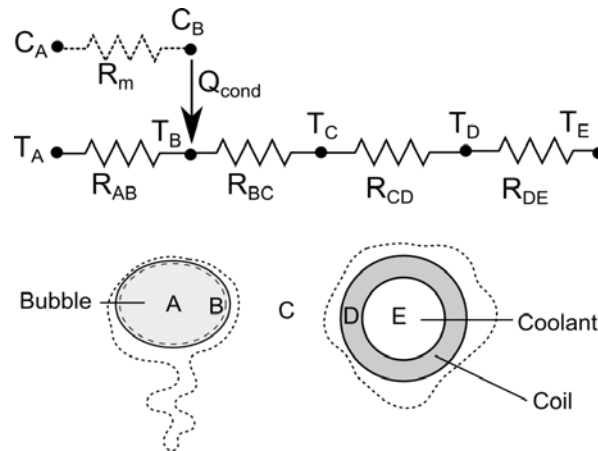

Figure 2: Resistance network from [12] governing heat and mass transfer in the liquid region of a bubble column dehumidifier, with resistances (R), mean concentrations (C) and mean temperatures (T). Node B is just inside the bubble surface. C_B is a saturated state at T_B.

The resistance model of Figure 2 is included to inform the derivation of the maximum single-stage heat transfer rate that will be discussed in Section 3.2 and to enable discussion of the experimental results in terms of the relative magnitudes of the resistances. In developing the resistance network, conduction resistance through the (thin copper) coil wall is neglected. In addition, R_{BC} is found to be significantly smaller than the other resistors, and will not be discussed in this paper [12].

In columns where the coolant tubing passes through the air gap above the column liquid, additional heat is transferred outside the column that is not governed by the resistance network of Figure 2. When the bubbles coalesce at the liquid surface, they become a stream of moist air which transfers both latent and sensible heat to the tubing as it flows to the air outlet. The heat transferred to the tubing is then transferred to the coolant, and the condensation which forms on the tubing falls into the column liquid.

3.2   Maximum Heat Transfer Rate of a Single Stage

This section will model the maximum steady heat transfer rate of a single bubble column stage, which is the heat transfer rate to the coolant that would be expected if there was zero resistance to heat or mass transfer. The column liquid is expected to be so well-mixed by the rising bubbles that it can be modeled as isothermal [5]. Neglecting heat transfer in the air gap above the liquid, the column can be treated as two single-stream devices in contact with the isothermal column liquid: a heat exchanger on the coolant side, and a simultaneous heat and mass exchanger on the bubble side [12]. To maintain a steady column temperature, Equation 1 dictates that the heat transfer rate into the fluid from the moist air, including the latent heat added at the bubble surface by condensation, must be equal to the heat transferred into the coolant:

$$\dot{Q}_{max//} = \dot{Q}_{DE} = \dot{Q}_{AB} + \dot{Q}_{cond} \tag{1}$$

Applying conservation of energy to the two streams gives the heat transfer rates as a function of inlet and outlet enthalpies and mass flow rates, as shown in Equations 2-4:

$$\dot{Q}_{DE} = \dot{m}_E [h_f(T_{E,o}) - h_f(T_{E,i})] \tag{2}$$

$$\dot{Q}_{AB} = \dot{m}_a [h_a(T_{A,i}) - h_a(T_{A,o})] + \dot{m}_{w,o}[h_g(T_{A,i}) - h_g(T_{A,o})] + \dot{m}_{cond}[h_g(T_{A,i}) - h_g(T_B)] \tag{3}$$

$$\dot{Q}_{cond} = \dot{m}_{cond} h_{fg}(T_B) \tag{4}$$

The maximum heat transfer rate in a single column stage occurs when the air and coolant both exit at the temperature of the column liquid, as in Equation 5. The bubble surface temperature is also assumed to equal the column temperature.

$$T_{E,o} = T_{A,o} = T_B = T_C \tag{5}$$

The inlet and outlet water vapor mass flow rates and the dry air mass flow rate are related by Equations 6-8. The inlet water vapor mass fraction assumes a saturated state at the inlet temperature.

$$\dot{m}_a = \dot{m}_{ma}(1 - m_i) \tag{6}$$

$$\dot{m}_{w,i} = \dot{m}_{ma} m_i \tag{7}$$

$$\dot{m}_{w,o} = \dot{m}_{w,i} - \dot{m}_{cond} \tag{8}$$

The calculation of maximum heat transfer rate will assume the exiting bubbles are saturated, as shown in Equation 9:

$$\frac{P_{sat}(T_{A,o})}{P} = \frac{\dot{m}_{w,o}}{\dot{m}_{w,o} + (M_g/M_a)\dot{m}_a} \tag{9}$$

All properties are evaluated at atmospheric pressure because the pressure drop is small for these short (4-21 cm) bubble columns which are open to the atmosphere and which have approximately hydrostatic pressure profiles [5]. These equations, combined with definitions of mass fraction, mole fraction, etc. are used to calculate the maximum possible heat transfer rate within the liquid part of a single bubble column stage. Engineering Equation Solver (EES), which has built-in functions for fluid properties such as enthalpy, was used to solve this set of equations [14].

3.3   Parallel-Flow Effectiveness

Narayan et al. proposed a model for the effectiveness of simultaneous heat and mass exchangers by which bubble columns can be compared to other dehumidifier types, which are generally counterflow [15]. Compared to counterflow dehumidifiers, the effectiveness of a single-stage bubble column dehumidifier is low because the device functions as if it is in parallel-flow regardless of the coil and bubble stream orientations due to the interaction of both streams with the well-mixed column liquid.
This leads to the need for multi-stage devices. Narayan and Lienhard [3] demonstrated that combining bubble column stages at different liquid temperatures into a multi-staged device with an overall counterflow configuration can achieve effectiveness comparable to conventional dehumidifiers.

However, effective multi-staging requires each stage of the column to have a low enthalpy pinch [16]. As a performance parameter, enthalpy pinch represents an improvement over temperature pinch because of the nonlinearity of the enthalpy-temperature curve of saturated moist air, but it is still a dimensional quantity. Good heat recovery requires that each stage achieve a large fraction of its maximum single-stage heat transfer rate. Therefore, to compare the effects of design and operational parameters of a single column stage, a parallel-flow effectiveness, $\varepsilon_{//}$, is defined. Equation 10 gives $\varepsilon_{//}$ as a function of the actual and maximum possible heat transfer rates of a single, well-mixed stage, as defined by Equations 1-9.

$$\varepsilon_{//} = \frac{\dot{Q}_{meas}}{\dot{Q}_{max//}} \tag{10}$$

Changes to the column design and operation will be analyzed in terms of both heat flux—the heat transfer rate per submerged coil surface area—and parallel-flow effectiveness to capture effects on both capital and energy costs. Because only single-stage bubble columns are considered in this paper, all further references to "effectiveness" will mean the parallel-flow effectiveness, $\varepsilon_{//}$.

IV.   METHODS

Heat flux and parallel-flow effectiveness are measured for a variety of coil lengths, air temperatures, and column liquid heights.

4.1   Experimental Apparatus

Dehumidifier heat flux and effectiveness are measured with an instrumented HDH system. The dehumidifier is 28 cm square by 36 cm high, but can be filled to any desired liquid height. The temperature and flow rate of moist air and the coolant flow rate are adjustable. The experimental dehumidifier, including the locations of the five thermocouples, is shown in Figure 1.

Moist air enters the dehumidifier from a humidifier, in which compressed dry air is forced through a porous stainless steel cartridge sparger into a tank heated by a submerged resistance heater. The moist air leaves the humidifier close to saturation, and it cools slightly as it passes through insulated rubber tubing and a rotameter to the dehumidifier. Condensation in the rotameter verifies that the air entering the dehumidifier is saturated.

The effect of condensation in the rotameter on the flow rate reading was neglected, but the difference in density of the hot, moist air from the dry air at STP for which the rotameter is calibrated was accounted for. Since gas flow in a rotameter is largely inviscid, the flow rate is proportional to the square root of the density, leading to the correction factor in Equation 14:

$$\frac{\dot{V}_{actual}}{\dot{V}_{reading}} = \sqrt{\frac{\rho_{a,STP}}{\rho_{ma}(T_{A,i})}} \tag{14}$$

All cooling coils were made from 9.5 mm OD copper tubes. The two larger coils had an 8.5 cm turn radius, while the smallest (8.7 cm long, 26 cm^2) "coil" had a turn radius of approximately 16 cm. For reference, the largest coil used here (900 cm^2) was comparable in length and equivalent in diameter to the coils used by Narayan et al. [5]. The vertical part of each coil, which connects the immersed portion to the chilled water source, was covered by 3.2 mm thick, 9.5 mm ID rubber tubing that had been slit along the side and wrapped around the copper tube to provide some insulation.

The 20 cm square orifice-plate sparger used in the dehumidifier had 64 holes, each 2.83 mm in diameter.

4.2   Experimental Parameters

The design and operational parameters varied in this experiment are listed in Table 1 in the Appendix along with the three dependent variables (T_C, $T_{E,o}$, and $T_{A,o}$) used in data analysis. In each trial, the humidifier and chiller were brought to the desired operating temperatures. The column and coil were configured as desired, and the humid air and chilled water were allowed to flow through the column at the desired flow rates. After observing that T_C, $T_{E,o}$, and $T_{A,o}$ had reached relatively steady values, all temperatures were recorded.

Although the column was insulated with 2.5 cm thick open-cell foam sheets, some heat may have been lost to the environment. Heat loss would tend to raise the enthalpy loss of the air and lower the enthalpy gain of the coolant. Additionally, gradual fluctuations in humidifier and coolant temperature made it difficult to ensure that the column had reached a steady temperature. Small deviations from a steady column liquid temperature would also have opposite effects on the coolant and moist air streams. Therefore, heat transfer rate was found from the average enthalpy change of the coolant and moist air

streams. The heat transfer rate into the coolant, $\dot{Q}_{meas,E}=\dot{Q}_{DE,}$ is found with Equation 2. The heat transfer rate to the column from the air, $\dot{Q}_{meas,A}$, is computed from the change in enthalpy of the moist air stream with Equation 15.

$$\dot{Q}_{meas,A} = \dot{m}_a[h_a(T_{A,i}) - h_a(T_{A,o})] + \dot{m}_{w,o}[h_g(T_{A,i}) - h_g(T_{A,o})] + \dot{m}_{cond}[h_g(T_{A,i}) - h_g(T_C) + h_{fg}(T_C)] \qquad (15)$$

To solve Equation 15, the water vapor mass flow rates must be related by continuity (Equation 8). Equation 16 can be solved for the outlet mass flow rate, assuming the outlet air is saturated at the measured outlet temperature:

$$\frac{P_{sat}(T_{A,o})}{P} = \frac{\dot{m}_{w,o}}{\dot{m}_{w,o} + (M_g/M_a)\dot{m}_a} \qquad (16)$$

The actual heat transfer rate effectiveness was then calculated from the average of the two heat transfer rate measurements, $\dot{Q}_{meas,E}$ and $\dot{Q}_{meas,A}$. The heat flux was computed as the ratio of actual heat transfer rate to outer surface area of coil immersed in the column liquid, and effectiveness was computed with Equation 10.

V.   RESULTS

The effects of variations in coil surface area, air inlet temperature, and column liquid height on heat flux and parallel-flow effectiveness are demonstrated in this section. The additional heat transfer that occurs in the air gap above the column liquid is discussed. For completeness, and because some variables such as coolant temperature were difficult to control, all raw experimental data are listed in the appendix (Table 1).

5.1   Coil Area

The relationship between coil area and parallel-flow effectiveness is clear, but even more marked is the effect of coil area on heat flux. Figure 3 shows these trends.
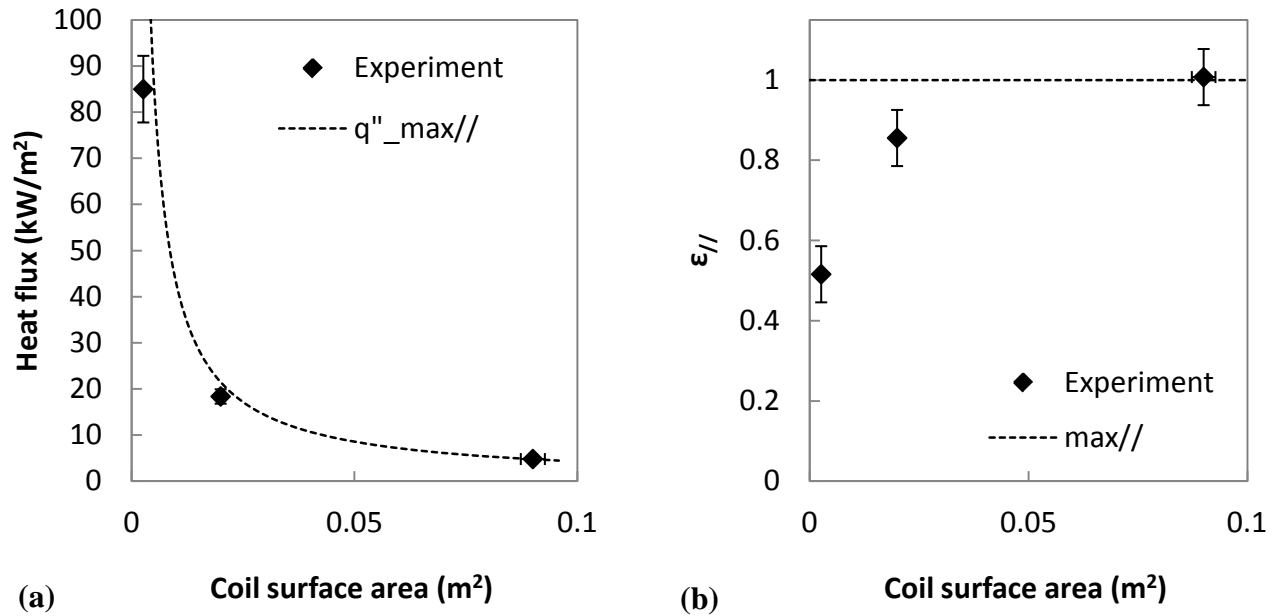
Figure 3: Effect of coil area on (a) heat flux and (b) effectiveness.

Effectiveness increases with coil area, asymptotically approaching a value near one. Although a value of one is within the margin of error for the measured parallel-flow effectiveness of the largest coil, the parallel-flow effectiveness can potentially exceed unity due to thermal interaction between the air and coolant streams in the air gap above the column liquid, which was neglected in the definition of $\varepsilon_{//}$ and is discussed in more detail in Section 5.4. The effect of coil surface area on effectiveness is not pronounced except at very small areas because the heat transfer rate is not strongly dependent on coil area and the maximum single-stage heat transfer rate is independent of coil size. Therefore, heat flux— the heat transfer rate per unit coil area—rises sharply as the coil size is minimized. Because the heat flux gained by minimizing coil area comes with a loss of effectiveness, the optimal coil area must be determined by analyzing the cost and performance of a complete HDH system.

5.2   Moist Air Temperature

The effects of varying moist air inlet temperature on heat flux and effectiveness are plotted in Figure 4.
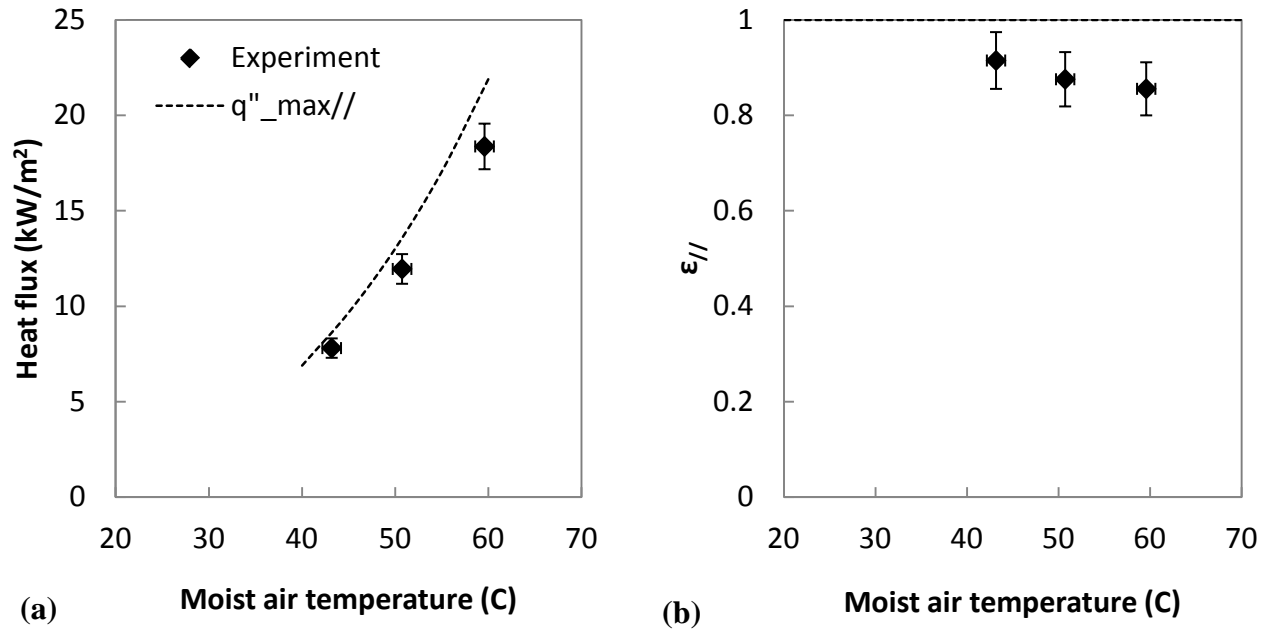
Figure 4: Effect of moist air temperature on (a) heat flux and (b) effectiveness.

Heat flux increases sharply with moist air temperature because both the higher concentration of condensable water vapor and the higher temperature contribute to the enthalpy of the warmer moist air. However, effectiveness decreases with increasing air temperature. Although the temperature difference across the coil increases with increasing air temperature, the maximum heat transfer rate increases to a greater degree due to the shape of the enthalpy-temperature curve of saturated moist air, which curves upward due to the increase in water vapor pressure with temperature. Because the maximum heat transfer rate rises faster than the temperature difference and the heat transfer coefficients of the coil are near-constant, the effectiveness decreases with increasing moist air temperature.

5.3   Column Liquid Height

Narayan et al. [5] found that heat flux was independent of liquid height for heights above 15 cm, the minimum height necessary to cover the cooling coil used in that work. They postulate that the critical height, above which heat flux is independent of height, is on the order of the bubble diameter [5]. In this paper, the coil had only one loop, and therefore the minimum height that could be tested was lower, about 4 cm. Liquid height was measured at the side of the column during bubbling. Figure 5 shows that for the 2.83 mm orifice plate and flow rate tested, the critical height is below 4 cm.
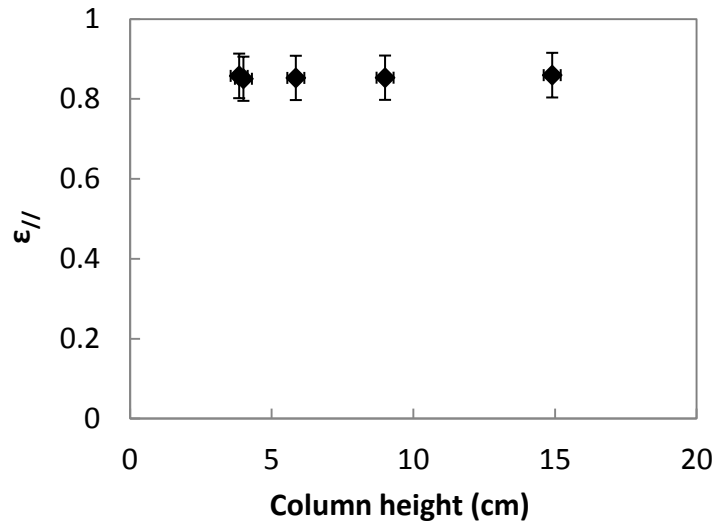
Figure 5: Effectiveness of varying column heights, showing that the critical height is below the minimum height necessary to cover the coil.

Above the height where the coil is covered (4 cm), column height has no measurable effect on effectiveness. The absence of any decrease in effectiveness at heights as low as 4 cm suggests that much of the heat transfer occurs early in each bubble's residence in the column while its inner temperature and concentration profiles are still developing. Although it is difficult to verify the claim of Narayan et al. [5] that the critical height is only a few millimeters, these results are consistent with that hypothesis.

Minimizing the liquid height will improve bubble column performance by reducing the hydrostatic contribution to the air inlet pressure, thereby reducing the power needed to pump the air. The result that the effectiveness is not diminished by reducing the height to 4 cm is fortunate, because the pressure drop (assuming hydrostatic head and, to be conservative, zero gas holdup) is only about 400 Pa per stage, or 2 kPa for a five-stage dehumidifier. Using narrower tubes to reduce the liquid height which just covers the coil further lowers the pressure drop, as shown by Narayan et al. [5] who demonstrated a three-stage bubble column dehumidifier with a gas-side pressure drop of just 800 Pa.

5.4   Air-Gap Heat Transfer

It is notable in Figure 3 that $\varepsilon_{//}$ can exceed unity in a column where the coolant tube passes through the air gap. This occurs because of additional heat transfer in the air gap above the column fluid, which is excluded from the model for the maximum heat transfer rate of a single stage. This additional heat transfer also explains the observation that the air tends to leave colder than the column liquid (see Table 1 in the Appendix). Figure 6 is a qualitative sketch of the temperature profiles of the coolant and air.
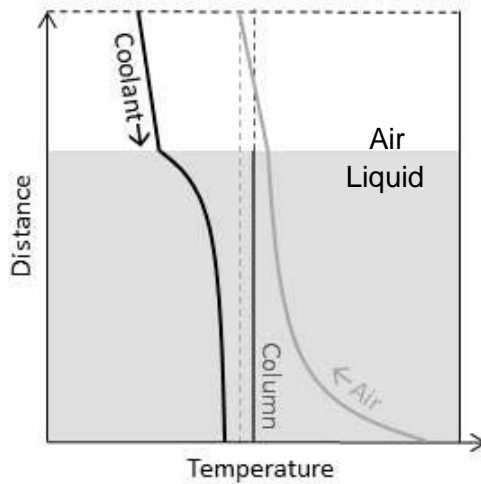
Figure 6: Coolant and moist air stream temperature profiles in a column showing the air leaving below the column liquid temperature.

The heat transfer rate in the gap was estimated by assuming that saturated air enters the gap at the temperature of the column liquid. The independence of effectiveness from column height supports this approximation. A similar system of equations to that used in Section 4.2 was solved with EES [14] to determine the heat transfer rate in the air gap. Figure 7 expresses the air gap heat transfer rate as a fraction of the total heat transfer rate, which is in this case also calculated from the air stream. The fraction ranges between 5-40% but tends to be smaller when the temperature pinch is small.
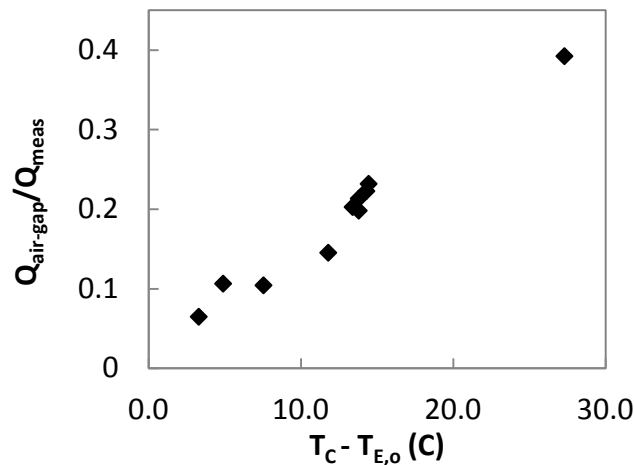

Figure 7: The fraction of heat transfer occurring in air gap increases with the liquid-side temperature pinch.

Figure 7 shows that the fraction of heat transfer occurring in the air gap increases with the liquid-side temperature pinch, T_C-$T_{E,o}$. It is likely that if the vertical section of tubing were not insulated, the fraction of heat transfer occurring in the air gap would be greater. In practice, with columns designed to have a low temperature pinch, the fraction of heat transfer occurring outside the column is expected to be small. In columns with no exposed coolant tubing, the air gap heat transfer rate should be negligible.

However, exposing a section of tubing in the air gap may be beneficial if it is compatible with the column design.

VI. CONCLUSIONS

Experiments were performed to enhance understanding of the factors influencing bubble column dehumidifier performance. A parallel-flow effectiveness was defined to complement the heat flux when describing the performance of a single-stage bubble column dehumidifier. The heat flux can be raised dramatically by reducing the coil area, but this gain is offset by a loss of effectiveness. Increasing air temperature leads to increased heat flux but decreased effectiveness. Liquid height should be minimized because effectiveness is independent of liquid height above the height necessary to cover the single-loop coil. Additional heat transfer in the air gap is found to increase with liquid-side temperature pinch. These findings will inform the design of bubble column dehumidifier stages with short coils for high heat recovery and low capital cost.

VII. ACKNOWLEDGEMENT

VIII. REFERENCES

1. Ettouney, H. Design and analysis of humidification dehumidification desalination process, Desalination 183(1-3) (2005) 341-352
2. Narayan, G. P., McGovern, R. K., Thiel, G. P., Miller, J. A., Sharqawy, M. H., Zubair, S. M., Antar, M. A., Lienhard V, J. H. Status of humidification-dehumidification desalination, Proceedings of the IDA World Congress on Desalination and Water Reuse, Perth, Australia (2011)
3. Narayan, G. P., St. John, M. G., Zubair, S. M., Lienhard V, J. H. Thermal design of the humidification dehumidification desalination system: An experimental investigation, International Journal of Heat and Mass Transfer, 58(1–2) (2013) 740-748
4. Narayan, G. P., Sharqawy, M. H., Lienhard V, J. H., Zubair, S. M. Thermodynamic analysis of humidification dehumidification desalination cycles, Desalination and Water Treatment, 16(1-3) (2010) 339-353
5. Narayan, G. P., Sharqawy, M. H., Lam, S., Das, S. K. Lienhard V, J. H. Bubble columns for condensation at high concentrations of non-condensable gas: heat transfer model and experiments, AIChE Journal 59(5) (2013) (1780-1790)
6. Klausner, J.F., Mei, R., Li, Y. Innovative fresh water production process for fossil fuel Plants, U.S. DOE - Energy Information Administration annual report (2003)
7. Narayan, G.P. and Lienhard V, J.H., Thermal design of humidification dehumidification systems for affordable small-scale desalination, IDA Journal, 4(3) (2012) 24-34
8. Kantarci, N., Borak, F., Ulgen, K. O. Review: Bubble column reactors, Process Biochemistry, 40(7) (2005) 2263–2283

9. Leibson, I., Holcomb, E.G., Cacoso, A. G., Jacmic, J. J. Rate of flow and mechanics of bubble formation from single submerged orifices II: Mechanics of bubble formation, AIChE Journal, 2(3) (1956) 300-306

10. Joshi, J.B., Shah, Y.T. Invited Review: Hydrodynamic and mixing models for bubble column reactors, Chemical Engineering Communications, 11(1-3) (1981) 165-199

11. Akita, K., Yoshida, F. Bubble size, interfacial area, and liquid-phase mass transfer coefficient in bubble columns, Industrial & Engineering Chemistry Process Design and Development, 13(1) (1974) 84-91

12. Tow, E. W., Lienhard V, J. H. Analytical modeling of a bubble column dehumidifier, Proceedings of the ASME Summer Heat Transfer Conference, Minneapolis, MN, accepted for presentation in July, 2013

13. Barrett, E. C., Dunn, S. G. Design of direct contact humidifiers and dehumidifiers using tray Columns, Industrial & Engineering Chemistry Process Design and Development, 13(4) (1974) 353-358

14. Klein, S.A. Engineering Equation Solver. F-Chart Software, LLC

15. Narayan, G. P., Mistry, K. H., Sharqawy M. H., Syed M. Zubair, S. M., Lienhard V, J. H. Energy effectiveness of simultaneous heat and mass exchange devices, Frontiers in Heat and Mass Transfer 1(2) (2010) 1-13

16. Narayan, G. P., Chehayeb, K. M., McGovern, R. K., Thiel, G. P., Zubair, S. M., Lienhard V, J. H. Thermodynamic balancing of the humidification-dehumidification desalination system by mass extraction and injection, International Journal of Heat and Mass Transfer, 57(2) (2013) 756-770

APPENDIX: RAW DATA

Many factors affect the performance of the experimental dehumidifier. Care was taken to keep all independent variables except for the variable(s) of interest constant across all runs in each plot. However, some were difficult to control. Table 1, which contains all design parameters and raw data collected in this experiment, is included for completeness and to allow the reader to draw his or her own conclusions. All trials used a coolant flow rate of 8.3 mL/s. All air temperature measurements were dry bulb measurements. Dependent variables are marked with an asterisk.

Table 1: Raw Data

$\dot{V}_{ma}$ (L/s)	$T_{E,i}$ (°C)	$T_{E,o}$ (°C)*	$T_{mq,i}$ (°C)	$T_{ma,o}$ (°C)*	T_C (°C)*	A_{coil} (cm^2)	Height (cm)	Figure	$\varepsilon_{//}$*
1.56	19.9	24.7	59.6	46.0	52.0	26	10	3, 7	0.516
1.56	19.8	32.7	59.6	33.4	36.0	900	10	3, 7	1.007
1.56	20.0	30.3	59.6	37.8	42.1	200	10	3, 4, 7	0.856
1.49	20.7	25.3	43.2	28.2	30.2	200	10	4, 7	0.915
1.52	20.0	26.7	50.8	31.5	34.2	200	10	4, 7	0.876
2.01	16.3	30.7	58.4	39.8	45.0	200	4	5, 7	0.858
2.01	16.6	30.6	58.4	39.5	45.0	200	4	5, 7	0.851
2.01	16.7	30.7	58.3	39.4	44.5	200	6	5, 7	0.853
1.97	16.4	30.3	58.3	39.3	44.1	200	9	5, 7	0.853
1.99	17.0	30.9	58.4	39.4	44.3	200	15	5, 7	0.860